Results in Chemistry 19 (2026) 102914

Contents lists available at ScienceDirect

Results in Chemistry

journal homepage: www.sciencedirect.com/journal/results-in-chemistry

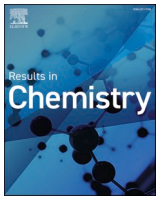

A physico-chemical insight into the benzaldehyde reduction mechanism catalysed by CdS/TiO_2 composites activated by visible light

Martina Milani [a], Giuliana Magnacca [b,*], Maria Carmen Valsania [b], Edoardo Marchini [a], Alessandra Molinari [a]

[a] Università degli Studi Ferrara, Dipartimento di Scienze chimiche, farmaceutiche ed agrarie, Via Luigi Borsari 46, 44121 Ferrara, Italy
[b] Università degli Studi di Torino, Dipartimento di Chimica e NIS Interdepartmental Centre, Via Pietro Giuria 7, 10125 Torino, Italy

ARTICLE INFO

Keywords:
CdS/TiO_2 composites
Heterojunctions
Surface properties
Band energetics
Aldehyde photocatalytic reduction

ABSTRACT

CdS/TiO_2 1/n ($n = 4$, 8 and 32) composite materials are synthesized maintaining constant the amount of CdS and varying the amount of TiO_2. XRD, HRTEM, FESEM/EDS analysis point out that both CdS and TiO_2 maintain their original crystalline structure but are in intimate interconnection. BET and porosity analysis evidence that SSA are similar in all cases, with *CdS/TiO_2 1/32* showing also mesoporosity in addition to microporosity. Microcalorimetric analysis demonstrates that all composite materials are hydrophilic in nature, but *CdS/TiO_2 1/8* and *CdS/TiO_2 1/32* show a larger number of sites interacting with water molecules. Photoelectrochemical investigation showed that the intimate contact between CdS and TiO_2, allows electrons injection from CdS to TiO_2 increasing the lifetimes of separated charges. Cyclic voltammetry experiments demonstrate that both CdS and TiO_2 can reduce benzaldehyde with electrons residing in their conduction bands, whereas the surface features of the composite favor the photocatalyst/substrate interactions. The understanding of how to combine energetics, heterojunctions, morphology and surface characteristics of the photoactive materials opens the way towards an efficient design of *CdS/TiO_2 1/n* composite systems, which show significant advances over the use of the two separate components: i) the presence of TiO_2 modifies the characteristics of the CdS surface, favouring the approach of organic molecules, such as benzaldehyde and its reaction intermediates; ii) CdS, activated by irradiation with visible light, can inject electrons onto TiO_2 which is in turn activated without using UV light. This paves the way for the application of more sustainable experimental conditions to achieve reductive transformations in the presence of TiO_2.

1. Introduction

Illumination of suspended semiconductors has emerged to be an option available technology for photocatalytic reactions, such as wastewater treatment [1], fuel production (e.g. H_2) through water splitting [2] and redox (i.e. oxidative and reductive) chemical transformations [3]. What keeps research interest in photocatalysis high is the possibility to use solar energy, which is the purest, most abundant and completely renewable source of energy.

Titanium dioxide (TiO_2) is the most popular semiconductor in heterogeneous photocatalysis, and it has been extensively investigated [4–6]. The reasons for its tremendous success are its high photocatalytic efficiency, robustness, chemical stability, low toxicity, low cost and environmental friendliness. Although research on TiO_2 has focused more on its pronounced oxidizing properties fuelling knowledge in the field of environmental remediation and oxidation of pollutant and non-pollutant molecules [7], TiO_2 has also attracted interest as a photocatalyst in reduction processes carried out in the absence of oxygen. In fact, by UV light excitation, it is able to reduce nitro-aromatic compounds to the corresponding anilines [8–15], to catalyse the reductive cleavage of N═N bonds in azodyes [16] and to transform aromatic aldehydes into alcohols [17–20].

Despite the extensive research on TiO_2-based photocatalysis, it is necessary to recall the two main disadvantages of this semiconductor, that limit its use in photocatalysis and in solar photocatalysis [21]: first, because of its very wide band gap (3.2 eV), photoactivation of TiO_2 occurs with UV light, which accounts for about 5 % of the solar spectrum. Second, photogenerated electrons and holes in the bulk of TiO_2

* Corresponding author.
E-mail addresses: martina.milani@unife.it (M. Milani), giuliana.magnacca@unito.it (G. Magnacca), mariacarmen.valsania@unito.it (M.C. Valsania), edoardo.marchini@unife.it (E. Marchini), alessandra.molinari@unife.it (A. Molinari).

https://doi.org/10.1016/j.rechem.2025.102914
Received 2 September 2025; Accepted 25 November 2025
Available online 2 December 2025

coexist in the same particle, and their migration to the surface to initiate a redox process competes with recombination, which remains a high probability reaction. As a result, the number of desired chemical events is significantly smaller than that expected considering the light energy absorbed.

To overcome these limitations, several approaches have been proposed and put into the field in the research literature. To increase solar energy utilization by extending the wavelength of TiO_2 photoactivation into the visible region of the spectrum, photosensitization, grafting of metal complexes, doping with metal ions and non-metal elements are the most studied strategies [22–26]. In addition, electron/hole recombination can be lowered by the fabrication of appropriate heterojunctions between two semiconductors in intimate contact: lifetimes of separated charges are longer, thus allowing more charge carriers to diffuse to the surface [27–30].

Cadmium sulfide (CdS), with a band gap of only 2.4 eV, is a material that responds to visible light. It is characterized by good charge mobility, which allows photogenerated electrons and holes to reach the surface in a timely manner, promoting redox reactions on its surface. However, CdS suffers from poor photostability and undergoes severe photocorrosion that limits its efficiency [31].

The coupling of CdS with TiO_2 has attracted great interest because this mixed system offers, at once, a possible solution to the main disadvantages of TiO_2, having the capacity of absorbing solar visible light and the ability to separate photoexcited electrons and holes. In fact, band structures of the two materials are matched: the conduction band of CdS is located at potentials more negative than that of TiO_2 [32,33], and visible irradiation of CdS allows electron injection from the chalcogenide to dark TiO_2 while photogenerated holes remain in the valence band of CdS. Some of us have recently demonstrated that spatially separation of charges on two different materials causes an increase in the lifetimes of electrons and holes, favouring their transfer to acceptors and donors, so enhancing the photocatalytic activity with respect to the single materials alone [34]. In addition, it is generally reported that the presence of TiO_2 improves the photostability of CdS [35–40]. Based on the above considerations of band energetics, it can be hypothesized that the CdS/TiO_2 composite system is able of performing all the photocatalytic transformations previously explored for UV light-activated TiO_2 alone, with the advantage brought by the presence of CdS, that the material can be activated with visible light.

In the present study, a series of *CdS/TiO_2 1/n* composite materials were synthesized, keeping the amount of CdS constant and varying that of TiO_2. Prepared materials were physico-chemically and spectroscopically characterized by XRD, HRTEM, FESEM/EDS, BET and BJH method, adsorption microcalorimetry, IR, UV–vis spectroscopies and used in the photocatalytic reduction of benzaldehyde to benzyl alcohol with visible light. Despite favourable energetics, CdS was unable to successfully carry out the reaction and the presence of TiO_2 was necessary to restore the photocatalytic activity. We show that the amount of TiO_2 determines surface characteristics that are closely related to photocatalytic activity, demonstrating that band energetics is one of the factors to be considered but not the only factor on which photocatalytic activity depends, especially when dealing with surface redox processes at the solid-liquid interface.

2. Materials and methods

2.1. Preparation of colloidal CdS nanoparticles

A stable aqueous colloidal solution of nanoparticles of cadmium sulfide was obtained by the method of chemical condensation [36,41]. In brief, water solutions of $CdCl_2$ (12.5 mM), Na_2S (12.5 mM), and EDTA (12.5 mM) were prepared and then mixed in equal volumes (10 mL) by shaking at room temperature for some minutes. When the overall solution was subjected to shaking, the EDTA-anions formed amphiphilic, negatively charged shells that made CdS Quantum Dots (QDs) water-soluble. The solution obtained had a yellow colour. Stable colloidal CdS QDs played the role of crystal seeds for nucleation and formation of anatase TiO_2 and remained well dispersed.

2.1.1. Preparation of colloidal CdS/TiO_2 1/n composites

In situ doping of amorphous TiO_2 by CdS QDs was carried out following a reported direct hydrolysis route [36,41]. Specifically, to aqueous colloidal solution of CdS (10 mL, 0.125 mmol) a measured amount of $Ti(OiPr)_4$ was slowly added (0.15, 0.3, and 1.2). Hydrolysis occurs. Then, samples were heated up to 90 °C under continuous stirring and aged at this temperature for 60′.

Later on, water slowly evaporated, and the recovered yellowish powders were rinsed with ethanol and water and then dried in the oven overnight under aerated conditions. Three different photocatalysts have been prepared: *CdS/TiO_2–1/4* (0.15 mL), *CdS/TiO_2–1/8* (0.3 mL), and *CdS/TiO_2–1/32* (1.2 mL). Commercial anatase TAA1 (Alfa Aesar) were used as reference for characterization purposes.

2.2. Catalysts characterization

X-Ray diffraction was used to determine the crystalline phases of the materials. The measurements were carried out using a X'Pert PRO MPD from PANalytical in Bragg−Brentano geometry diffractometers, using Cu Kα radiation (45 kV/40 mA) and a flat sample-holder. The XRD pattern acquisition was performed in the 2θ range of 20–80° with 0.03° interval step and 20 s per step to improve the signal-to-noise ratio.

High-Resolution Transmission Electron Microscopy (HRTEM) and Field Emission Scanning Electron Microscopy (FESEM) equipped with Energy Dispersive Spectroscopy microprobe (EDS) were used to evidence the presence and distribution of CdS and TiO_2 in the catalyst. HRTEM was JEOL 300 kV, FESEM was Tescan S9000G microscope. For FESEM/EDS analysis, the powder was metallized with a chromium layer of about 15 nm thickness.

BET surface area and DFT pore size distribution curves were obtained by N_2 gas-volumetric adsorption at 77 K using ASAP2020 (Micromeritics). All samples were treated in vacuo (residual pressure of 10^{-2} mbar) at 80 °C for several hours before the adsorption experiments to remove atmospheric contaminants from the surface and inside the pores. The treatment was long enough to maintain a good vacuum also in static condition (without assistance of the pumping system).

The hydrophilicity of the samples was evaluated by means of adsorption microcalorimetry using water vapor in contact with the sample activated in vacuo at 30 °C and kept at 30 °C along the measurement timespan. Adsorption microcalorimeter is equipped with a vacuum line with known volumes allowing the activation of the sample with a turbomolecular pump (residual pressure 10^{-5} mbar) and the contemporary admission of the vapor in the sample cell. In the vacuum line the absolute pressures are measured with a capacitive gauge. As all the volumes of the vacuum line are known, the reading of vapor pressures and temperatures, before and after the interaction with the adsorbing sample, allows to evaluate the adsorbed amounts by application of the perfect gas law and to build up the adsorption isotherms. In addition, the sample cell is inserted in the microcalorimeter together with an empty reference cell to evaluate the heats of adsorption released (which are exothermic) eliminating all the other thermal phenomena not related to the adsorption process.

Infrared spectra were recorded by a Nicolet 510P FTIR instrument in KBr, fitted with a Spectra-Tech collector diffuse reflectance accessory (range 4000 to 200 cm^{-1}). Powders were kept in the oven at 50 °C for a couple of days before the recording of the spectra. Other IR measurements were carried out on samples *CdS/TiO_2 1/4* and *1/32*. The same quantity of powders was suspended in CH_3CN/EtOH (4/1) mixture containing benzaldehyde (8×10^{-3} M). The suspension was stirred in the dark for five hours. Then, after centrifugation, the supernatant was removed and the powder dried in the oven overnight before the recording of the IR spectrum.

Absorption spectra of CdS/TiO_2 powders were collected under diffuse reflectance (R%) mode with a JASCO *V* 570 spectrophotometer equipped with an integrating sphere. For the band gap calculation, Tauc Plot analysis was applied according to (F(R) x hn)α = A x (hn – Eg) where α =1/2 for an indirect band gap and α =2 for a direct band gap, (F (R) = (1 − R)2/2R) is Kubelka-Munk function, A is a proportionality coefficient and Eg is the semiconductor band gap.

Cyclic voltammetry experiments were carried out using a Metrohm Autolab PGSTAT302N electrochemical workstation. For this type of analysis, the semiconductor was supported on a conductive glass substrate, specifically fluorine-doped tin oxide (FTO), following a previously reported procedure [12]. The measurements were performed in a three-electrode cell consisting of a saturated calomel electrode (SCE) as the reference electrode, a platinum wire as the counter electrode, and either FTO/TiO_2 or glassy carbon as the working electrode. Benzaldehyde (1×10^{-2} M) was dissolved in a CH_3CN/EtOH (4:1 *v*/v) mixture containing $TBAPF_6$ (0.1 M) as the supporting electrolyte. The solution was then transferred into the three-electrode electrochemical cell, which was sealed, and nitrogen was bubbled through the solution to remove dissolved oxygen.

2.3. Photocatalytic experiments

In a typical experiment, each *CdS/TiO_2 1/n* powder (3 g/L) was suspended in a CH_3CN/EtOH (4/1) mixture containing benzaldehyde (8×10^{-3}M) into a spectroscopic cell. The cell was closed and degassed by bubbling nitrogen for 30 min. The suspension is then illuminated for the desired period using a Xe/Hg lamp and λ > 420 nm cut-off filter. For comparison, the irradiation was performed with both benchmark TiO_2 (P25) and CdS. After irradiation the suspension was centrifuged twice, and the evolution of the reaction was monitored by GC-FID analysis, by using a HP-5 capillary column (30 m length, 0.32 mm internal diameter, 0.25 μm film thickness). The injection method was in gradient of temperature as follows: initial temperature 50 °C for 3 min, then 5 °C/min until 100 °C, and finally 100 °C for 10 min. The temperature of the injector and of the detector was 300 °C and the nitrogen flux was 2.5 mL/min. Pure benzaldehyde and benzyl alcohol solutions were used for qualitative and quantitative analysis. The conversion of aldehyde, the yield of benzyl alcohol, and the selectivity for alcohol were defined as follows:

$$Conversion\ (\%) = \frac{(C_0 - C_{aldehyde})}{C_0} x100$$

$$Yield\ (\%) = \frac{C_{alcohol}}{C_0} x100$$

$$Selectivity\ (\%) = \frac{C_{alcohol}}{(C_0 - C_{aldehyde})} x100$$

where C_0 is the initial concentration of benzaldehyde, $C_{aldehyde}$ and $C_{alcohol}$ are the concentrations of the substrate aldehyde and the corresponding alcohol, respectively, at a certain time after the photocatalytic reaction.

3. Results and discussion

3.1. Structural features of the samples

The diffractograms of the analyzed samples (Fig. 1) evidence the main signals of TiO_2 anatase phase in the expected intensity ratio reported for reference material (JCPDS card n. 00–021-1272, ref. [36] and Fig. S1). The width of the signals indicates the size of crystalline domains are very limited, as for nanocrystalline systems, but the half height width decreases while increasing the amount of TiO_2 in the composite material for the growth of anatase crystallites. The Debye-Scherrer

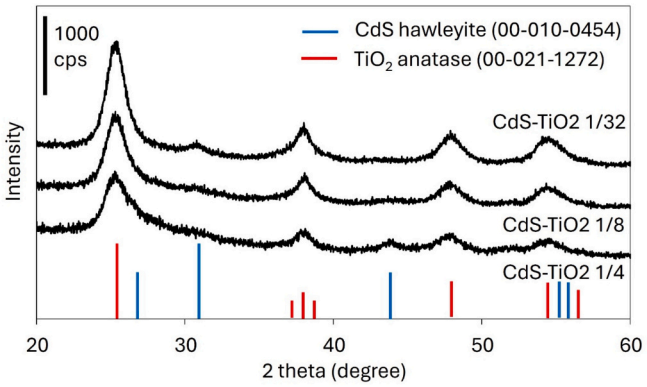

Fig. 1. X-Ray diffractograms of samples *CdS-TiO_2 1/4, CdS-TiO_2 1/8* and *CdS-TiO_2 1/32* compared with the main signals of CdS hawleyite in blue (reference card 00–010-0454) and TiO_2 anatase in red (reference card 00–021-1272). The diffractograms are shifted along the vertical axis for the sake of clarity. (For interpretation of the references to colour in this figure legend, the reader is referred to the web version of this article.)

calculation applied to the principal signal of anatase (2θ = 25.3°) in the three samples under investigation gives a size of the crystalline domains in the range 4–6 nm [XRD Crystallite (grain) Size Calculator (Scherrer Equation) - InstaNANO. https://instanano.com/all/characterization/xrd/crystallite-size/ (accessed May 7th, 2025)].

Only one signal at 2θ ≈ 31° reveals the presence of CdS, assignable to cubic hawleyite phase (JCPDS card n. 00–010-0454) which possesses an intense reflection in that position. However, the weak intensity of the peak suggests that the amount of CdS system is low in comparison with TiO_2 or that the CdS component is almost amorphous.

No traces of other phases are observable, indicating that CdS and TiO_2 maintain their original nature without forming other crystalline products. The shape of the curves and the width of the signals suggest the two compounds are not separated from each other but rather in intimate interconnection.

The intimate connection between the two compounds was also studied using the electron microscopy techniques HRTEM and FESEM hyphenated with an EDS probe. Fig. 2A reports the HRTEM images of *CdS-TiO_2 1/32*, i.e. the system that contains the largest amount of TiO_2 with the largest size of crystalline domains, as resulted from XRD investigation. The fringe pattern of 3.52 Å, observed in the micrographs, is in a very good agreement with anatase d_{101}, but unexpectedly the pattern of 3.36 Å is not assignable to TiO_2 and is, instead, in a good agreement with hawleyite d_{111} = 3.35 Å, indicating that also CdS is crystalline although the crystalline domains are very small. The nanoparticles, both CdS and TiO_2, are probably spherical, as there is no evidence of corners/edges or acicular shapes, and their size, corresponding to the size of the crystalline domains, does not overcome 10 nm.

The crystallites are mixed together, and the FESEM-EDS investigation evidences a homogeneous distribution of Ti, O, Cd and S elements in the materials (Fig. 2B). In addition, the molar ratio between the elements does not reflect the stoichiometry of the compounds: Ti/O ratio and Cd/S ratio results different than expected (1.152 rather than 0.5 for TiO_2 and 0.294 rather than 1 for CdS) confirming the intimate mixing of the two compounds, situation which is probably facilitated by the unit cell of the crystals, cubic for CdS hawleyite and tetragonal for TiO_2 anatase, and that should be highly beneficial for the photocatalytic activity of the systems.

3.2. Textural features of the samples

All the samples were tested for evaluating their specific surface area and porosity. These characteristics are very important when dealing with a heterogeneous photocatalyst, as in most parts of the cases the

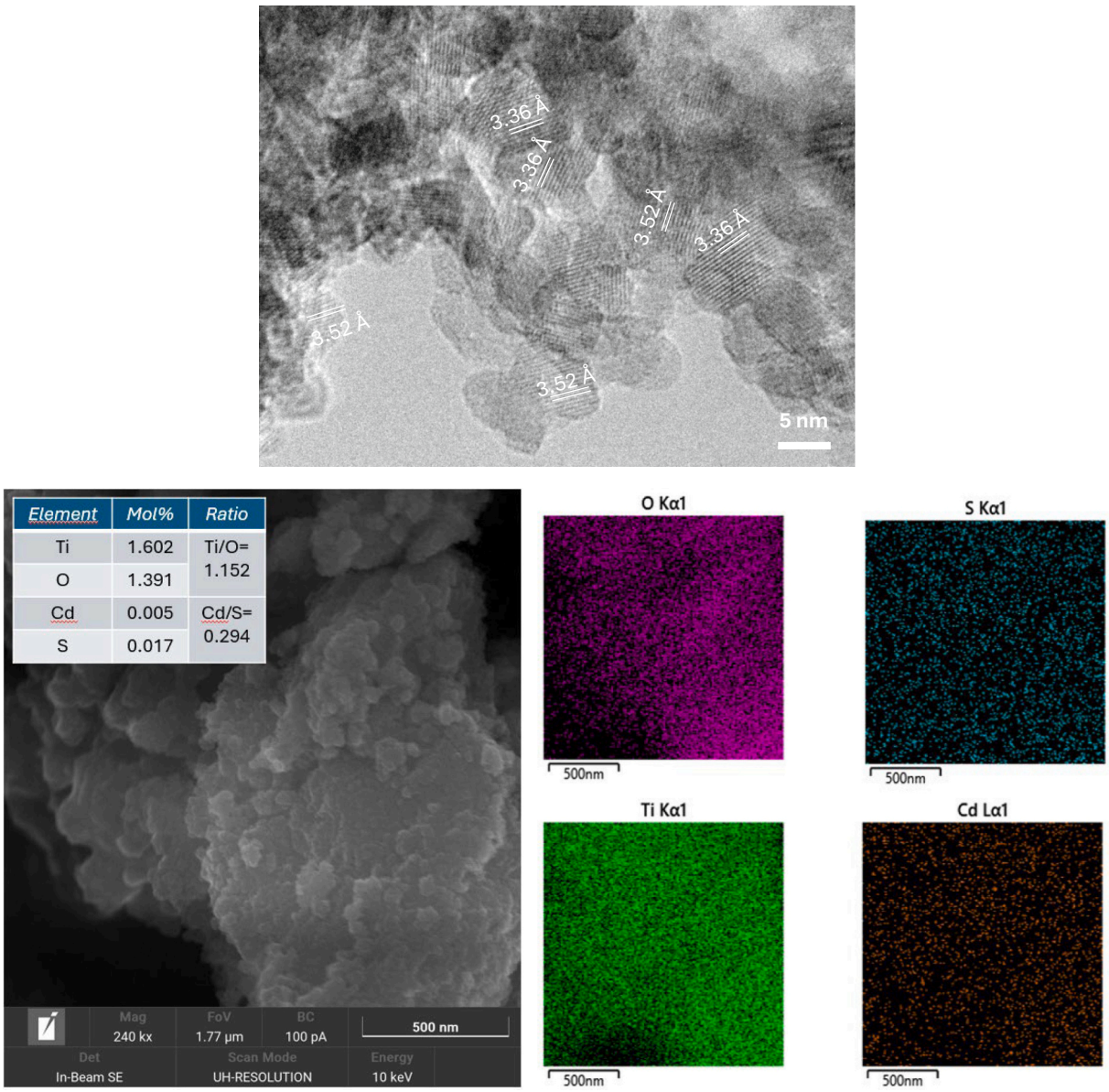

Fig. 2. A – HRTEM image of *CdS-TiO_2 1/32* evidencing the d_{hkl} values.
B – FESEM image of *CdS-TiO_2 1/32*, EDS elements mapping and relative amount of the elements.

photocatalytic activity is actuated at the level of the interface solid material/substrate. In fact, the irradiated solid material is expected to generate reactive species (electrons in the conduction band and positive vacancies in the valence band of the material) that need to be in intimate contact with the substrates to provoke their reaction. The specific surface area of materials can be enlarged if particles are porous, and in particular the presence of large size pores (at least in the range of mesopores, i.e. 2–50 nm of width) can promote the interaction material/substrate and the consequent reaction of the substrate.

The main results of N_2 adsorption at 77 K on the examined materials are reported in Fig. 3A (adsorption isotherms), 3B (pore size distribution curves) and Table 1 (specific surface area and pores volume). Table 1 and Fig. S2 also report the principal results related to reference commercial CdS and anatase TAA1 in order to evidence how the textural features of the two components are modified in the composite materials.

All isotherms are of the mixed type I-IV of the IUPAC classification, showing both a steep increase of the adsorbed amounts at very small values of relative pressures (typical of the presence of micropores) and a hysteresis loop (typical of mesoporous systems). The shape of the curves showing the change of slope at the beginning of the isotherms indicates that all the samples possess similar specific surface areas (a little smaller for the sample *CdS-TiO_2 1/8*). Otherwise, the width and height of the loops indicate that the sample *CdS-TiO_2 1/32* shows the largest number of large pores which are the most interesting for a real application of the materials, as substrates can be attracted and stably interact with the materials surface inside the pores improving the efficiency of the photocatalyst.

3.3. *Hydrophilicity of the samples*

The efficiency of a catalyst can be affected by the strength of the interaction catalyst/substrate and the nature of the surface is a key factor in determining the extent and ease of this interaction. As known, a polar substrate prefers a polar material; therefore, the polarity of the systems *CdS-TiO_2 1/n* was measured considering the number of water molecules (polar probe) adsorbed at the surface of the catalysts and the related energies of interaction as a function of coverage.

Fig. 4A reports the adsorption isotherms related to the three samples

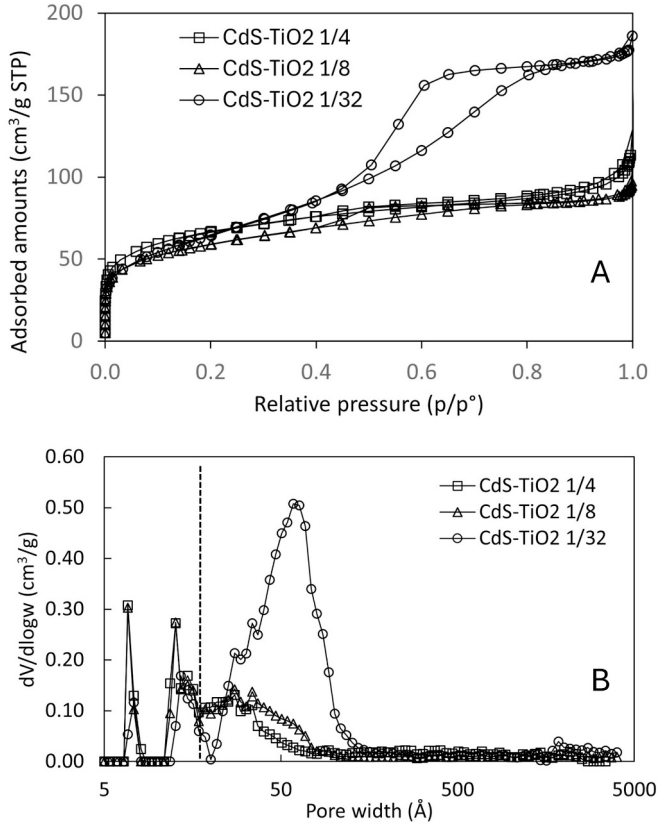

Fig. 3. – Section A: Adsorption-desorption N_2 isotherms carried out at 77 K on samples *CdS-TiO$_2$ 1/4* (squares), *CdS-TiO$_2$ 1/8* (triangles) and *CdS-TiO$_2$ 1/32* (circles) activated in vacuo at 80 °C. Section B: DFT pore size distribution curves related to the samples *CdS-TiO$_2$ 1/4* (squares), *CdS-TiO$_2$ 1/8* (triangles) and *CdS-TiO$_2$ 1/32* (circles) activated in vacuo at 80 °C. The broken vertical line represents the threshold value between micro and mesopores.

Table 1
BET specific surface area and pore volume of the samples *CdS-TiO$_2$ 1/4, CdS-TiO$_2$ 1/8* and *CdS-TiO$_2$ 1/32* and of the reference commercial CdS and anatase TAA1.

Sample	BET Surface Area (m^2/g)	DFT Total Pore Volume (cm^3/g)	DFT Micropore Volume (cm^3/g)	DFT Large pore Volume (cm^3/g)
CdS-TiO$_2$ 1/4	236	0.13	0.06	0.07
CdS-TiO$_2$ 1/8	210	0.13	0.05	0.08
CdS-TiO$_2$ 1/32	237	0.26	0.03	0.23
Commercial CdS	~ 1	< 0.01	–	< 0.01
Commercial TAA1	220	0.33	0.03	0.30

under investigation. The curves are expressed in µmol/m^2, i.e. considering the specific surface area of the samples and therefore expressing the affinity of water vapor for the sample surface eliminating the contribution of variable specific surface area of the compared samples. The data suggest a sharp change of the system behaviour increasing the ratio *CdS-TiO$_2$* from *1/4* to *1/8*, as the adsorbed amounts curves increase deeply for samples *CdS-TiO$_2$ 1/8* and *1/32*.

Although this modification of the surface properties is clear considering the adsorbed amounts, the heats of adsorption curves for all the materials remain in the same range, i.e. between 120 and 50 kJ/mol, and this suggests that the increase of hydrophilicity is only due to an increase of the number of the surface adsorbing sites than to a real

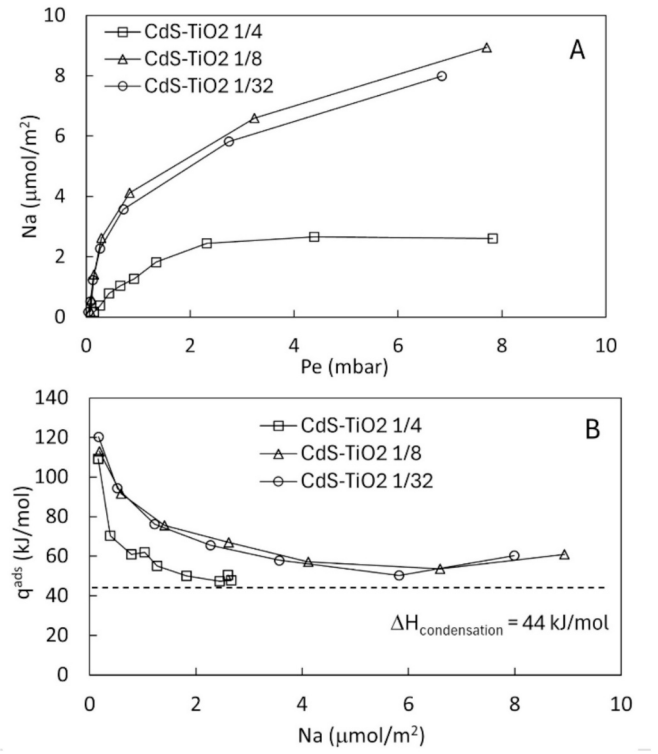

Fig. 4. – Adsorption isotherms (section A) and molar heats of adsorption curves (section B) related to the samples *CdS-TiO$_2$ 1/4* (squares), *CdS-TiO$_2$ 1/8* (triangles) and *CdS-TiO$_2$ 1/32* (circles) activated in vacuo at 30 °C. All the measurements were carried out keeping the samples at the constant temperature of 30 °C. The horizontal broken line in section B indicates the standard water condensation enthalpy considered as the threshold value between a hydrophilic and hydrophobic surface.

increase of the probe-surface interaction energy. In all samples the heats of adsorption are higher than the reference value of 44 kJ/mol (the water molar enthalpy of condensation), indicating that water molecules can interact with the materials surface with more than two H-bonds/molecule and therefore indicating that all the materials are strongly hydrophilic. The trend of the curves reported in Fig. 4B witnesses the heterogeneity of the adsorbing surfaces.

3.4. IR analysis

Fig. 5 reports IR spectra of the investigated composite powders *CdS-*

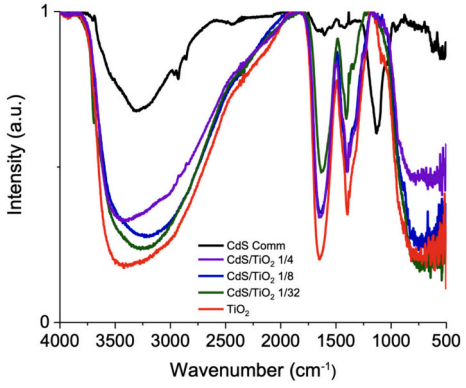

Fig. 5. FTIR spectra of *CdS-TiO$_2$ 1/4*, *CdS-TiO$_2$ 1/8* and *CdS-TiO$_2$ 1/32*. IR spectra of commercial CdS and of TiO_2 are reported for easy comparison. All the samples are dried in the oven at 50 °C for a couple of days before the recording of the spectrum.

TiO_2 1/4, CdS-TiO_2 1/8 and *CdS-TiO_2 1/32*, in comparison with commercial CdS and reference TiO_2. The spectra of pure CdS and TiO_2 are similar to those reported in the literature for similar materials and all the three composite samples have a spectrum profile relatable to that of TiO_2. Briefly, stretching vibrations of surface hydroxyl (-OH) groups interacting with each other and interacting with adsorbed water molecules via H-bonds are responsible for the broad peak at 3600–2000 cm^{-1}. The bending mode of water molecules adsorbed on the surface of the catalyst is responsible for the peak at 1628 cm^{-1} [42–44]. This signal seems to be over-imposed on other absorptions visible in the range 1800–1200 cm^{-1} assignable to the presence of carbonate/bicarbonate-like signals formed by interaction of the basic oxide with atmospheric CO_2, also involving -OH groups in the coordination sphere [45]. The strong absorption below 1000 cm^{-1} is related to the signal of Ti-O-Ti vibrations. The signal at 1100 cm^{-1}, characteristic of CdS material [46], is not visible in any of the composite systems, as the spectroscopic features of TiO_2 prevail on those of CdS.

Strong adsorptions due to the presence of OH groups and adsorbed water molecules confirm that the composite materials, as well as pure TiO_2, have a marked hydrophilic character, in accordance with microcalorimetric measurement suggestions. Also, the strong signals related to the interaction CO_2-surface indicate the presence of basic oxygen atoms at the surface of the materials and therefore confirm the polar nature of their surface.

In summary, the composite materials *CdS-TiO_2 1/4, CdS-TiO_2 1/8* and *CdS-TiO_2 1/32* show the physico-chemical features of the principal component titania anatase, whereas the presence of CdS in cubic arrangement (hawleyite phase) can be partially assessed by XRD results but surely proved by HRTEM images. Among all the composite materials, *CdS-TiO_2 1/32* is the most similar to pure anatase, being characterized by the strongest hydrophilicity and by the largest amount of mesopores.

3.5. Optical and photoelectrochemical properties

UV–vis diffuse reflectance spectra of TiO_2, CdS and the composite materials are shown in Fig. S3. As expected, the absorption of TiO_2 anatase ends at around 400 nm, while that of CdS extends deep into the visible region and ends at around 600 nm. Composite *CdS-TiO_2 1/n* show a significant absorption in the visible light range. Recorded spectra of the composite materials allowed the estimation of the band gap values of the two semiconductors by using the baseline method, as proposed by Macyk for multicomponent systems (in Fig. S4) [47]. Obtained values are reported in Table 2. The values are similar between samples, ranging between 3.2 and 3.3 eV for TiO_2 and 2.2–2.3 eV for CdS, confirming (like X-rays) that the intrinsic nature of the two components is intact.

From these data, it can be stated that the photoexcitation of *CdS/TiO_2 1/n* with visible light ($\lambda > 420$ nm) involves only the CdS component, in which charge separation occurs. The subsequent removal and transfer of photogenerated charges could take place in the heterojunction.

To improve understanding of this aspect, the key results obtained from previous photoelectrochemical investigations on FTO/TiO_2/CdS electrodes are summarized in the following [34,36].

A comparison between the emission spectra of FTO/CdS and FTO/TiO_2/CdS films shows that the latter displays a broadened spectrum, with a red shift of about 20 nm, that has been ascribed to some stabilizing interaction between CdS and TiO_2, which lowers the emission energy (Fig. S5).

Photovoltage decay experiments provide insights into the recombination dynamics of charge carriers obtained from the illumination of FTO/CdS and FTO/TiO_2/CdS systems (Fig. S6). In the case of FTO/CdS, turning off the light leads to a very rapid decay of the photovoltage, whereas with the FTO/TiO_2/CdS system, the decay occurs more slowly when dark conditions are restored. This indicates that electron transfer takes place between CdS and TiO_2, slowing down the charge recombination process [34,48].

A time-resolved fluorescence analysis of CdS/TiO_2 composite systems with different degrees of crystallinity was recently published [36]. To facilitate the collection of useful information, we report the main conclusions of this investigation (Fig. S7): the decay analysis revealed a distribution of sites from which radiative recombination of charges occurred with different rate constants and, in particular, a long-lived amplitude was observed, with a decay on a nanosecond timescale. Moreover, the emission tail observed with the more crystalline CdS/TiO_2 was attributed to the radiative recombination of electrons injected into TiO_2, with holes remaining in CdS. This indicates that intimate contact between CdS and TiO_2 should favor the dynamics of electron transfer.

In summary, visible light excitation of CdS in *CdS/TiO_2 1/n* systems causes charge separation and electron injection into the conduction band or trap states of dark TiO_2.

Since it is known that the relative position of the CdS and TiO_2 bands is such that it can generate a type II heterojunction, as occurs also with other couples of photoactive materials [49], we propose here a different approach. In detail, visible light is used to improve the photoactivity of CdS thanks to the characteristics of the composite system. We are well aware that the phenomena observed on short time scales (e.g. radiative recombination slowed down, injection of electrons from CdS to anatase, increase of lifetimes) are simply an indication in favor of improved photocatalysis, which often implies multielectron heterogeneous processes that occur on much longer time scales (milliseconds/s).

3.6. Photocatalytic reduction of benzaldehyde

The reaction chosen as a probe to investigate the photocatalytic properties of prepared *CdS-TiO_2 1/n* systems is the reduction of benzaldehyde to benzyl alcohol.

Dark cyclic voltammetry (0 *V*/−2.0 V vs SCE) was performed using a glassy carbon as working electrode in the presence of benzaldehyde (1×10^{-2} M) dissolved in CH_3CN/EtOH 4/1, with $TBAPF_6$ (0.1 M) as supporting electrolyte in the absence of oxygen. The voltammogram shows a main cathodic wave at −1.75 *V*, with an onset at a slightly less negative potential value (around −1.55 V). This can be assigned to the electrochemical reduction of benzaldehyde, considering that the wave is not observable in the absence of the molecule (Fig. S8).

In Fig. 6 (black curve) it is reported the CV curve with FTO/TiO_2 P25 as working electrode in the absence of benzaldehyde: the filling of trap states of P25 occurs at around −1.4 V while a more intense process, appearing at stronger negative polarization (−2.0 V), is assigned to electron acceptor states, likely corresponding to the conduction band of TiO_2. Interestingly, when benzaldehyde is present in solution (red curve), a shoulder at −1.75 V, likely relative to the aldehyde reduction, is observable. Moreover, trap states of P25 shift to less negative potential values, suggesting a possible interaction between benzaldehyde and TiO_2 surface. These results indicate that TiO_2 can reduce benzaldehyde.

Regarding the photocatalytic process of reduction of benzaldehyde to benzyl alcohol, we expect from the UV-vis absorption spectrum of TiO_2 that the material is not activated upon visible light illumination ($\lambda > 420$ nm), but only upon UV radiation [10]. However, considering the lower band gap of CdS (Table 2) and the relative position of its

Table 2
Band gap values of CdS and TiO_2 estimated in the composite materials *CdS-TiO_2 1/4*, *CdS-TiO_2 1/8* and *CdS-TiO_2 1/32*.

Sample	CdS (eV)	TiO_2 (eV)
CdS/TiO_2 1/4	2.33	3.37
CdS/TiO_2 1/8	2.29	3.32
CdS/TiO_2 1/32	2.29	3.28
TiO_2	/	3.27
CdS	2.31	/

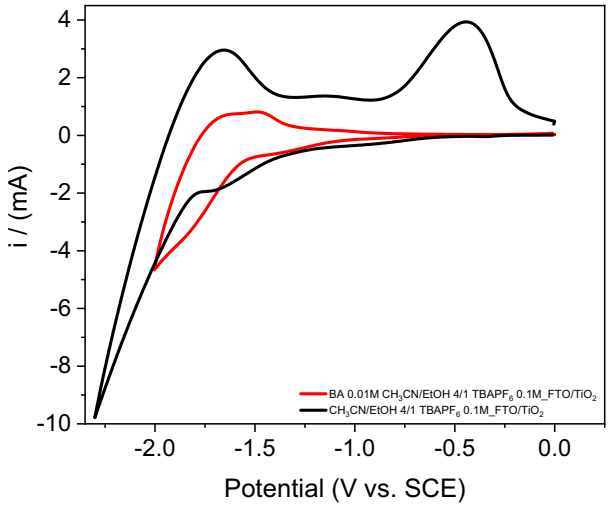

Fig. 6. Dark cyclic voltammetry in the presence (red line) or in the absence (black line) of benzaldehyde (BA, 1×10^{-2} M) in dearated CH_3CN/EtOH 4/1 solution, containing $TBAPF_6$ (0.1 M), recorded in the 0 V/−2.0 V range vs. SCE, using FTO/TiO_2 as the working electrode. The scan rate was set at 50 mV/s. (For interpretation of the references to colour in this figure legend, the reader is referred to the web version of this article.)

conduction band with respect to that of TiO_2 [32,33], we predict that under deaeration conditions, CdS would be able to catalyse this reaction, just as it can catalyse other reductive processes under photoexcitation with visible light [36,48,50].

For this, CdS was suspended in a CH_3CN/EtOH 4/1 mixture containing dissolved benzaldehyde. After deaeration, the suspension was illuminated (300 min) with wavelengths higher than 420 nm. At the end of the illumination period, the solution was separated from the photocatalyst, and the remaining benzaldehyde and the formed benzyl alcohol were quantified. Table 3 (1st column) shows that, unexpectedly, any conversion of benzaldehyde was obtained upon photoexcitation of CdS.

Analogous experiments were carried out with the composite *CdS/TiO_2 1/4*, *CdS/TiO_2 1/8* and *CdS/TiO_2 1/32*. The results are collected in Table 3. *CdS/TiO_2 1/4* has a very low activity. In contrast, *CdS/TiO_2 1/8* and *CdS/TiO_2 1/32* catalyse the reduction of benzaldehyde into the corresponding alcohol with increasing efficiency.

In fact, conversion is strongly associated with TiO_2 content: it increases by increasing the amount of TiO_2. Considering that the amount of CdS, which is the photoactive component, is kept constant in the composite systems, the different photocatalytic performances could depend on two factors, working in synergy: i) a more efficient charge separation and ii) textural modifications of the material.

This result is particularly important because it clearly shows that the reducing capability of a semiconductor depends on its conduction band position and is related to the morphology of the material. The interaction between the molecule to be transformed and the photocatalyst at the surface level is important in heterogeneous photocatalysis, especially when multielectronic processes are involved.

ATR measurements carried out with *CdS/TiO_2 1/4* and *CdS/TiO_2 1/32* before and after a period in contact with a benzaldehyde solution in the dark are reported in Figs. 7 and 8, respectively. In the case of *CdS/TiO_2 1/4*, no evident spectral changes are observed in the ATR spectrum after the contact. Probably, the weak interaction of benzaldehyde with the surface is the main factor determining the low photocatalytic activity obtained with this material (Table 3).

In contrast, the interaction of benzaldehyde with *CdS/TiO_2 1/32* is strong, as demonstrated by the drastic modification of the spectrum in the range 3250–750 cm^{-1} reported in Fig. 8. After benzaldehyde contact, several vibrational modes appear along the entire range of the spectrum, and several bands can be assigned to the vibrations of aldehydic and aromatic moieties ($\nu_{C\text{-}H}$ in the range 3100–2800 cm^{-1}, benzaldehyde $\nu_{C=O}$ at about 1700 cm^{-1} and vibrations of the ring with several weak-medium intensity signals in the range 1450–1150 cm^{-1}). The position of the signals expected for the molecule in the liquid phase shifts to lower wavenumbers, probably due to the interaction with the catalyst surface.

From all these observations, we conclude that the amount of TiO_2 in the surface of the photocatalysts has a role in determining the degree of interaction between benzaldehyde and the photocatalytic material *CdS/TiO_2 1/n*: in *CdS/TiO_2 1/4* the interaction is negligible, and this does not favor the reaction. By contrast, the reaction yield and aldehyde conversion clearly increased from *CdS/TiO_2 1/8* to *CdS/TiO_2 1/32*, i.e. when there was sufficient TiO_2 to ensure good interaction with benzaldehyde.

According to the results reported here and with the band positions of TiO_2 and CdS reported in literature [32,33], we propose the following mechanism for the reduction of benzaldehyde to benzyl alcohol with *CdS/TiO_2 1/n* systems (Scheme 1): upon visible light irradiation ($\lambda >$ 420 nm) electron-hole pairs are separated only on CdS, while TiO_2 is kept in the dark. Then, electrons can be injected from the CB of CdS to the CB of TiO_2, while holes remain localized on CdS. Ethanol acts as hole scavenger, undergoing oxidation and providing protons. Electrons and protons could carry out the multielectron reduction of benzaldehyde to the corresponding alcohol.

Table 3
Photocatalytic selective reduction of benzaldehyde into benzyl alcohol over *CdS/TiO_2 1/n* ($n = 4, 8, 32$) under visible light ($\lambda > 420$ nm). (n.e. indicates not evaluable).

After 300' Irradiation	CdS	CdS/TiO_2 1/4	CdS/TiO_2 1/8	CdS/TiO_2 1/32	TiO_2
Conversion (%)	n.e.	< 5	25.4	46.1	n.e.
Yield (%)	n.e.	< 5	10.6	25.0	n.e.
Selectivity (%)	n.e.	n.e.	42	54.2	n.e.

4. Conclusions

A series of *CdS/TiO_2 1/n* composite materials was synthesized by keeping the amount of CdS constant while varying the amount of TiO_2. Structural and morphological analysis (XRD, HRTEM, FESEM/EDS) point out that both CdS and TiO_2 maintain their original crystalline structure while forming intimate interconnection. BET and porosity analysis evidenced comparable surface areas across all samples, with *CdS/TiO_2 1/32* showing mesoporosity in addition to microporosity. Microcalorimetric analysis, using water as adsorbate, and IR

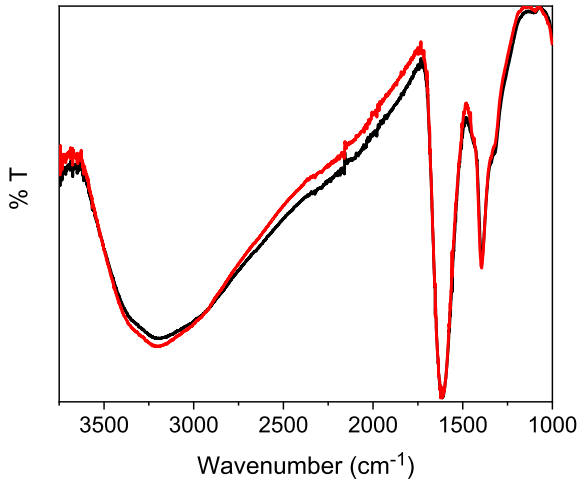

Fig. 7. ATR spectra of CdS/TiO_2 1/4 before (red) and after (black) the contact with benzaldehyde in the dark. (For interpretation of the references to colour in this figure legend, the reader is referred to the web version of this article.)

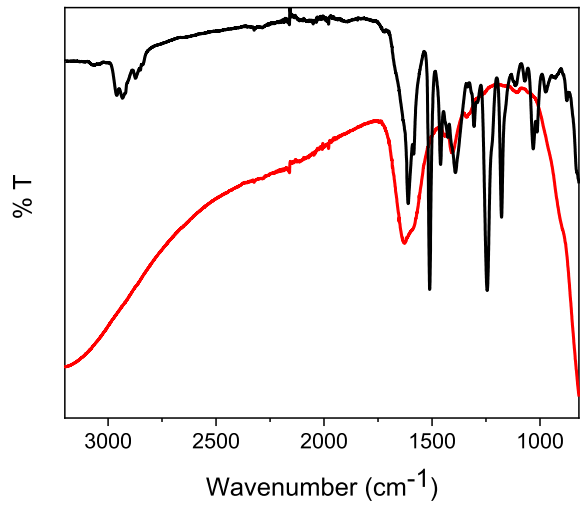

Fig. 8. ATR spectra of *CdS/TiO$_2$ 1/32* before (red) and after (black) the contact with benzaldehyde in the dark. (For interpretation of the references to colour in this figure legend, the reader is referred to the web version of this article.)

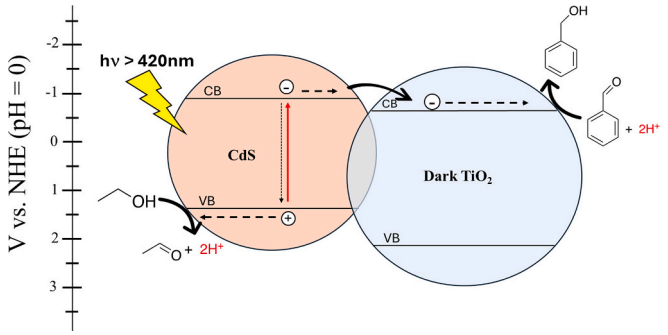

Scheme 1. Proposed photocatalytic mechanism occurring on *CdS/TiO$_2$ 1/8* and *1/32*

spectroscopy reveal that the three composite materials are hydrophilic in nature, but *CdS/TiO$_2$ 1/8* and *CdS/TiO$_2$ 1/32* show a larger number of interacting sites with respect to *CdS/TiO$_2$ 1/4*. ATR investigation demonstrates that benzaldehyde interacts with the surface of *CdS/TiO$_2$ 1/8* and *CdS/TiO$_2$ 1/32*. Furthermore, optical and photoelectrochemical measurements demonstrated efficient electron injection from CdS to TiO_2, resulting in longer lifetimes of separated charge carriers.

A proper combination of textural and optical properties leads to *CdS/TiO$_2$ 1/n* materials able to efficiently catalyse the visible-light-driven reduction of benzaldehyde to benzyl alcohol. *CdS/TiO$_2$ 1/8* and *CdS/TiO$_2$ 1/32* are photoactive, with a reaction yield that increases by increasing TiO_2 content in the composite system. By contrast, *CdS/TiO$_2$ 1/4* shows very low activity, despite being a composite material, consistent with its weak interaction with benzaldehyde as ATR analysis shows.

Overall, the rational design of CdS/TiO_2 1/n composite systems demonstrates the following: i) the presence of TiO_2 modifies the surface properties of CdS, increasing its hydrophilicity and facilitating interaction with organic molecules such as benzaldehyde and its reaction intermediates; ii) CdS acts as the sole photoactive component and subsequent electron transfer to TiO_2 through the heterojunction enables utilization of visible light instead of UV light. The combination of suitable morphological and optical properties paves the way for revisiting TiO_2-based reductive transformations performed using UV light but under more sustainable (visible-light-driven) conditions.

CRediT authorship contribution statement

Martina Milani: Visualization, Validation, Methodology, Investigation, Data curation. **Giuliana Magnacca:** Writing – review & editing, Writing – original draft, Validation, Investigation, Conceptualization. **Maria Carmen Valsania:** Methodology, Investigation. **Edoardo Marchini:** Methodology, Investigation. **Alessandra Molinari:** Writing – review & editing, Writing – original draft, Validation, Supervision, Funding acquisition, Conceptualization.

Declaration of competing interest

The Authors declare that they have no known competing financial interests or personal relationships that could have appeared to influence the content of this paper.

Acknowledgements

This work was supported by the University of Ferrara [FIRD 2024]. The authors GM and MCV acknowledge support from Project CH4.0 under MUR (Italian Ministry for the University) program “Dipartimenti di Eccellenza 2023-2027” (CUP: D13C22003520001).

Appendix A. Supplementary data

Supplementary data to this article can be found online at https://doi.org/10.1016/j.rechem.2025.102914.

Data availability

Data will be made available on request.

References

[1] S.N. Ahmed, W. Haider, Heterogeneous photocatalysis and its potential applications in water and wastewater treatment: a review, Nanotechnology 29 (2018) 342001, https://doi.org/10.1088/1361-6528/aac6ea.
[2] G. Colón, Towards the hydrogen production by photocatalysis, Appl. Catal. A Gen. 518 (2016) 48–59, https://doi.org/10.1016/j.apcata.2015.11.042.
[3] G. Palmisano, V. Augugliaro, M. Pagliaro, L. Palmisano, Photocatalysis: a promising route for 21st century organic chemistry, Chem. Commun. (2007) 3425–3437, https://doi.org/10.1039/B700395C.
[4] Q. Guo, Z. Ma, C. Zhou, Z. Ren, X. Yang, Single molecule Photocatalysis on TiO_2 surfaces: focus review, Chem. Rev. 119 (2019) 11020–11041, https://doi.org/10.1021/acs.chemrev.9b00226.
[5] A. Fujishima, X. Zhang, D. Tryk, TiO_2 photocatalysis and related surface phenomena, Surf. Sci. Rep. 63 (2008) 515–582, https://doi.org/10.1016/j.surfrep.2008.10.001.
[6] K. Nakata, A. Fujishima, TiO_2 photocatalysis: design and applications, J Photochem Photobiol C: Photochem Rev 13 (2012) 169–189, https://doi.org/10.1016/j.jphotochemrev.2012.06.001.
[7] H. Choi, S.R. Al-Abed, D.D. Dionysiou, E. Stathatos, P. Lianos, TiO_2-based advanced oxidation nanotechnologies for water purification and reuse, Sustain.Sci. Engin. 2 (2010) 229–254, https://doi.org/10.1016/S1871-2711(09)00208-6.
[8] J.L. Ferry, W.H. Glaze, Photocatalytic reduction of nitro organics over illuminated titanium dioxide: role of the TiO_2 surface, Langmuir 14 (1998) 3551–3555, https://doi.org/10.1021/la971079x.
[9] H. Kominami, S. Iwasaki, T. Maeda, K. Imamura, K. Hashimoto, Y. Kera, B. Ohtani, Photocatalytic reduction of nitrobenzene to aniline in an aqueous suspension of titanium(IV) oxide particles in the presence of oxalic acid as a hole scavenger and promotive effect of dioxygen in the system, Chem. Lett. 38 (2009) 410–411, https://doi.org/10.1246/cl.2009.410.
[10] Y. Shiraishi, Y. Togawa, D. Tsukamoto, S. Tanaka, T. Hirai, Highly efficient and selective hydrogenation of Nitroaromatics on Photoactivated rutile titanium dioxide, ACS Catal. 2 (2012) 2475–2481, https://doi.org/10.1021/cs300500p.
[11] A. Hakki, R. Dillert, D. Bahnemann, Photocatalytic conversion of nitroaromatic compounds in the presence of TiO_2, Catal. Today 144 (2009) 154–159, https://doi.org/10.1016/j.cattod.2009.01.029.
[12] A. Molinari, A. Maldotti, R. Amadelli, Probing the role of surface energetics of electrons and their accumulation in Photoreduction processes on TiO_2, Chem. - A Eur. J. 20 (2014) 7759–7765, https://doi.org/10.1002/chem.201402039.
[13] A. Molinari, A. Maldotti, R. Amadelli, Effect of the electrolyte cations on photoinduced charge transfer at TiO_2, Catal. Today 281 (2017) 71–77, https://doi.org/10.1016/j.cattod.2016.09.008.

[14] A. Molinari, M. Mazzanti, M. Fogagnolo, Photocatalytic selective reduction by TiO_2 of 5-Nitrosalicylic acid ethyl Ester: a mild route to Mesalazine, Catal. Lett. 150 (2020) 1072–1080, https://doi.org/10.1007/s10562-019-02993-3.
[15] K. Imamura, K. Nakanishi, K. Hashimoto, H. Kominami, Chemoselective reduction of nitrobenzenes having other reducible groups over titanium(IV) oxide photocatalyst under protection-, gas-, and metal-free conditions, Tetrahedron 70 (2014) 6134–6139, https://doi.org/10.1016/j.tet.2014.04.067.
[16] M. Mazzanti, S. Caramori, M. Fogagnolo, V. Cristino, A. Molinari, Turning waste into useful products by Photocatalysis with Nanocrystalline TiO_2 thin films: reductive cleavage of azo bond in the presence of aqueous Formate, Nanomaterials 10 (2020) 1–17, https://doi.org/10.3390/nano10112147.
[17] S. Kohtani, E. Yoshioka, K. Saito, A. Kudo, H. Miyabe, Adsorptive and kinetic properties on photocatalytic hydrogenation of aromatic ketones upon UV irradiated polycrystalline titanium dioxide: differences between Acetophenone and its Trifluoromethylated derivative, J. Phys. Chem. C 116 (2012) 17705–17713, https://doi.org/10.1021/jp3056174.
[18] S. Kohtani, Y. Kamoi, E. Yoshioka, H. Miyabe, Kinetic study on photocatalytic hydrogenation of acetophenone derivatives on titanium dioxide, Catal, Sci. Technol. 4 (2014) 1084–1091, https://doi.org/10.1039/C3CY00879G.
[19] M. Fukui, H. Kouda, A. Tanaka, K. Hashimoto, H. Kominami, Heterogeneous Meerwein-Ponndorf-Verley–type reduction of aromatic aldehydes having other reducible functional groups over a TiO_2 Photocatalyst, Chem.Select 2 (2017) 2293–2299, https://doi.org/10.1002/slct.201602018.
[20] M. Fukui, A. Tanaka, K. Hashimoto, H. Kominami, Meerwein–Ponndorf–Verley-type reduction over a metal-free TiO_2 Photocatalyst in alcohol: Chemoselective hydrogenation of Chlorobenzaldehyde to Chlorobenzyl alcohol, Chem. Lett. 45 (2016) 985–987, https://doi.org/10.1246/cl.160476.
[21] J.A. Rengifo-Herrera, C. Pulgarin, Why five decades of massive research on heterogeneous photocatalysis, especially on TiO_2, has not yet driven to water disinfection and detoxification applications? Critical review of drawbacks and challenges, Chem. Eng. J. 477 (2023) 146875, https://doi.org/10.1016/j.cej.2023.146875.
[22] R. Amadelli, L. Samiolo, A. Maldotti, A. Molinari, D. Gazzoli, Selective Photooxidation and Photoreduction processes at TiO_2 surface-modified by grafted Vanadyl, Int. J. Photoenergy 2011 (2011) 259453, https://doi.org/10.1155/2011/259453.
[23] S. Kohtani, S. Nishioka, E. Yoshioka, H. Miyabe, Dye-sensitized photo-hydrogenation of aromatic ketones on titanium dioxide under visible light irradiation, Catal. Commun. 43 (2014) 61–65, https://doi.org/10.1016/j.catcom.2013.09.006.
[24] G. Rossi, L. Pasquini, D. Catone, A. Piccioni, N. Patelli, A. Paladini, A. Molinari, S. Caramori, P. O'Keeffe, F. Boscherini, Charge carrier dynamics and visible light photocatalysis in vanadium-doped TiO_2 nanoparticles, Appl. Catal. B Environ. 237 (2018) 603–612, https://doi.org/10.1016/j.apcatb.2018.06.011.
[25] J. Choi, H. Park, M.R. Hoffmann, Effects of single metal-ion doping on the visible-light Photoreactivity of TiO_2, J. Phys. Chem. C 114 (2010) 783–792, https://doi.org/10.1021/jp908088x.
[26] L. Samiolo, M. Valigi, D. Gazzoli, R. Amadelli, Photo-electro catalytic oxidation of aromatic alcohols on visible light-absorbing nitrogen-doped TiO_2, Electrochim. Acta 55 (2010) 7788–7795, https://doi.org/10.1016/j.electacta.2009.09.044.
[27] H. Yu, H. Irie, K. Hashimoto, Conduction band energy level control of titanium dioxide: toward an efficient visible-light-sensitive photocatalyst, J. Am. Chem. Soc. 132 (2010) 6898–6899, https://doi.org/10.1021/ja101714s.
[28] Y. Chen, J.C. Crittenden, S. Hackney, L. Sutter, D.W. Hand, Preparation of a novel TiO_2-based p−n junction nanotube photocatalyst, Environ. Sci. Technol. 39 (2005) 1201–1208, https://doi.org/10.1021/es049252g.
[29] S. Lettieri, M. Pavone, A. Fioravanti, L. Santamaria Amato, P. Maddalena, Charge carrier processes and optical properties in TiO_2 and TiO_2-based heterojunction photocatalysts: A Review, *Materials,* 14, (2021), 1645, Doi: https://doi.org/10.3390/ma14071645.
[30] B.T. Barrocas, N. Ambrožová, K. Kočí, Photocatalytic reduction of carbon dioxide on TiO_2 heterojunction photocatalysts-a review, Materials 15 (2022) 967, https://doi.org/10.3390/ma15030967.
[31] L. Cheng, Q. Xiang, Y. Liao, H. Zhang, CdS-based photocatalysts, Energy Environ. Sci. 11 (2018) 1362–1391, https://doi.org/10.1039/C7EE03640J.
[32] R. Marshall, Semiconductor composites: strategies for enhancing charge carrier separation to improve photocatalytic activity, Adv. Funct. Mater. 24 (2014) 2421–2440, https://doi.org/10.1002/adfm.201303214.
[33] L. Zheng, F. Teng, X. Ye, H. Zheng, X. Fang, Photo/electrochemical applications of metal sulfide/TiO_2 Heterostructures, Adv. Energy Mater. 10 (2020) 1902355–1902386, https://doi.org/10.1002/aenm.201902355.
[34] M. Mazzanti, M. Milani, V. Cristino, R. Boaretto, A. Molinari, S. Caramori, Visible light reductive photocatalysis of azo-dyes with n–n junctions based on chemically deposited CdS, Molecules 27 (2022) 2924, https://doi.org/10.3390/molecules27092924.
[35] N. Qutub, P. Singh, S. Sabir, S. Sagadevan, W.-C. Oh, Enhanced photocatalytic degradation of acid blue dye using CdS/TiO_2 nanocomposite, Sci. Rep. 12 (2022) 5759, https://doi.org/10.1038/s41598-022-09479-0.
[36] M. Milani, M. Mazzanti, S. Caramori, G. Di Carmine, G. Magnacca, A. Molinari, Composite CdS/TiO_2 powders for the selective reduction of 4-Nitrobenzaldehyde by visible light: relation between preparation, Morphology and Photocatalytic Activity, Catalysts 13 (2022) 74, https://doi.org/10.3390/catal13010074.
[37] S. Liu, N. Zhang, Z.-R. Tang, Y.-J. Xu, Synthesis of One-Dimensional CdS@TiO_2 Core–Shell Nanocomposites Photocatalyst for Selective Redox: The Dual Role of TiO_2 Shell, ACS Appl. Mater. Interfaces 4 (2012) 6378–6385, https://doi.org/10.1021/am302074p.
[38] S. Bai, H. Li, Y. Guan, S. Jiang, The enhanced photocatalytic activity of CdS/TiO_2 nanocomposites by controlling CdS dispersion on TiO_2 nanotubes, Appl. Surf. Sci. 257 (2011) 6406–6409, https://doi.org/10.1016/j.apsusc.2011.02.007.
[39] A. Meng, B. Zhu, B. Zhong, L. Zhang, B. Cheng, Direct Z-scheme TiO_2/CdS hierarchical photocatalyst for enhanced photocatalytic H_2-production activity, Appl. Surf. Sci. 422 (2017) 518–527, https://doi.org/10.1016/j.apsusc.2017.06.028.
[40] H. Park, H.-H. Ou, U. Kang, J. Choi, M.R. Hoffmann, Photocatalytic conversion of carbon dioxide to methane on TiO_2/CdS in aqueous isopropanol solution, Catal. Today 266 (2016) 153–159, https://doi.org/10.1016/j.cattod.2015.09.017.
[41] A.S. Vorokh, N.S. Kozhevnikova, T.I. Gorbunova, O.I. Gyrdasova, I.V. Baklanova, L. Y. Buldakova, M.Y. Yanchenko, A.M. Murzakaev, E.V. Shalaeva, A.N. Enyashin, Facile, rapid and efficient doping of amorphous TiO_2 by pre-synthesized colloidal CdS quantum dots, J. Alloys Compd. 706 (2017) 205–214, https://doi.org/10.1016/j.jallcom.2017.02.235.
[42] G.J. de A.A. Soler-Illia, A. Louis, C. Sanchez, Synthesis and characterization of mesostructured Titania-based materials through evaporation-induced self-assembly, Chem. Mater. 14 (2002) 750–759, https://doi.org/10.1021/cm011217a.
[43] J.C. Yu, L. Zhang, Z. Zheng, J. Zhao, Synthesis and characterization of phosphated mesoporous titanium dioxide with high photocatalytic activity, Chem. Mater. 15 (2003) 2280–2286, https://doi.org/10.1021/cm0340781.
[44] R. Nakamura, A. Imanishi, K. Murakoshi, Y. Nakato, In situ FTIR studies of primary intermediates of photocatalytic reactions on Nanocrystalline TiO_2 films in contact with aqueous solutions, J. Am. Chem. Soc. 125 (2003) 7443–7450, https://doi.org/10.1021/ja029503q.
[45] L. Mino, G. Spoto, A.M. Ferrari, CO_2 capture by TiO_2 Anatase surfaces: a combined DFT and FTIR study, J. Phys. Chem. C 118 (2014) 25016–25026, https://doi.org/10.1021/jp507443k.
[46] K. Erturk, S. Isik, O. Aras, Y. Kaya, Investigation of structural, spectral, optical and nonlinear optical properties of nanocrystal CdS: electrodeposition and quantum mechanical studies, Optik 243 (2021) 167469–167479, https://doi.org/10.1016/j.ijleo.2021.167469.
[47] P. Makuła, M. Pacia, W. Macyk, How to correctly determine the band gap energy of modified semiconductor photocatalysts based on UV–vis spectra, J. Phys. Chem. Lett. 9 (2018) 6814–6817, https://doi.org/10.1021/acs.jpclett.8b02892.
[48] M. Milani, M. Mazzanti, C. Stevanin, T. Chenet, G. Magnacca, L. Pasti, A. Molinari, CdS-based hydrothermal photocatalysts for complete reductive dehalogenation of a chlorinated propionic acid in water by visible light, Nanomaterials 14 (2024) 579–594, https://doi.org/10.3390/nano14070579.
[49] F. Quin, Y. Xia, D. Yang, T. Xiao, X. Zhu, W. Feng, Z. Qui, Enhanced photocatalytic activity of g-C_3N_4/Bi_2WO_6 heterojunction via Z-scheme charge-transfer mechanism, J. Mol. Struct. 1346 (2024) 139023–139033, https://doi.org/10.1016/j.molstruc.2024.139023.
[50] M. Milani, M. Mazzanti, G. Magnacca, S. Caramori, A. Molinari, A novel hydrothermal CdS with enhanced photocatalytic activity and Photostability for visible light hydrogenation of azo bond: synthesis and characterization, Nanomaterials 13 (2023) 413–429, https://doi.org/10.3390/nano13030413.